CHAPTER 2

Regime Shifts

Regime shifts [**97**, **35**] are large and sudden changes in the structure or function of an ecosystem due to external disturbances. The term originates with observed changes in an ecosystem that are seen as signaling a drastic shift in the quality of ecosystem services [**16**]. Commonly cited examples of ecosystem regime shifts include the eutrophication of shallow lakes [**12**, **98**] due to increased nutrient loading, the collapse of fisheries due to overfishing [**19**, **20**], degradation of coral reefs due to seasonal hurricanes [**57**, **80**, **58**], and desertification due to climate change [**23**, **33**]. Human communities rely on the services these ecosystems provide; especially with regard to food, fiber, and air/water purification. Regime shifts can disrupt the quality of these services to a degree that is catastrophic for those dependent communities. There is, therefore, tremendous interest in finding ways to more accurately forecast and manage impending ecosystem regime shifts.

Ecosystem scientists have proposed a number of statistical indices for detecting impending regime shifts. These indices include Fisher information [**75**], increased variance [**95**], critical slowing [**18**], and conditional heteroskedasticity [**100**]. Experiments on food webs in whole lakes suggest these indices strengthen prior to the occurrence of a regime shift [**11**] , but these methods make little use of prior dynamical models and so it is unclear how to set detection thresholds for a meaningful false alarm rate. Moreover, these statistical indices provide little insight into the mechanisms driving a system towards a shift, and without such a mechanistic model it becomes unclear how one can develop policies that reliably forestall the occurrence of an impending regime shift. As a result, some have begun to question the practical value of the concept in adaptive resource management [43].

Ecologists often describe regime shifts in multi-stable systems as a transition between two stable equilibria. This viewpoint was popularized by Scheffer et al. in [97]. Fig. 2 graphically illustrates an *equilibrium-based* regime shift in which the system state jumps between the Regions of Attraction (ROA) of alternative *stable* equilibria. While the principles in Fig. 2 are easily grasped, there are several scenarios that do not easily fit into this picture. There are living systems [37], for example, that shift from a stable equilibrium to a limit cycle associated with an *unstable* equilibrium. Other living systems [92] exhibit "bursting" where the system repeatedly cycles between an oscillatory burst and fixed point convergence. Do we view this as switching back and forth between two distinct regimes or simply a single complex regime? One may also find dynamical systems that have no stable equilibria and yet they appear to have a steady state limit cycle that asymptotically approaches a collection of heteroclinic orbits [117]. Do the heteroclinic orbits represent distinct regimes or is the limit cycle a regime? The preceding scenarios suggest that the original equilibrium-based notion of a regime shift popularized by Scheffer et al. [97] is not sufficiently general to describe the full range of behaviors seen in living systems.

This chapter uses a simple model for lake eutrophication [12] to identify two regime shift mechanisms; *bifurcation-induced* and *shock-induced* regime shifts. We then use more realistic compartmental models [62] of lake eutrophication to show that real-life systems exhibit behaviors that do not fit into the equilibrium-based notion of a regime shift. This observation provides the motivation for introducing the concept of a *non-equilibrium regime shift* in which regimes are defined with respect to the components (also known as *basic sets*) of a Morse decomposition of the system's chain recurrent set.

1. Regime Shift Mechanisms for Shallow Lake Eutrophication

The equilibrium-based regime shift model for shallow lake eutrophication [12] was tremendously influential because it provided ecologists with a concrete way to visualize the mechanisms triggering a regime shift. This section reviews that regime shift model for lake eutrophication and uses it to identify two regime shift mechanisms that we call a *bifurcation-induced* and *shock-induced* regime shift. These two mechanisms may be distinguished by the time scale of the external disturbances triggering the regime shift. Shock-induced shifts are triggered by an impulsive disturbance whose time scale is much shorter than the primary time scale of the original process. In general, these shifts are triggered by "shocks" to the system that cause the system state to "jump" into an alternative regime. Bifurcation-induced shifts, on the other hand, are triggered by a disturbance whose time scale is much longer than the primary time scale in the original process. These shifts are triggered when a slowly drifting system parameter causes a structural shift (a.k.a. bifurcation) in the system flow field. This section describes these regime shift mechanisms with respect to eutrophication in shallow lakes.

Shallow lakes are bodies of fresh water that do not thermally stratify in the summer months [94]. These lakes are most highly prized in a pristine state where the biota is diverse and the water is clean and clear. Nutrients such as nitrogen and phosphorus play an essential role in the health of such lakes, but excessive nutrient levels (also known as *nutrient loading*) significantly degrade lake health by triggering algae blooms. Nutrient loads triggering such blooms often occur when nutrient enriched runoff flows into the lake from farm fields and cities . The appearance of such algae blooms is called *eutrophication*. The water in a eutrophic lake shifts from a clear to a turbid state; turbidity being caused by the lake biota being dominated by a single organism, i.e. algae. The resulting loss in biodiversity has a significant negative impact on lake ecosystem services (food, fiber, and clean water).

Eutrophication of fresh water lakes may cascade into larger downstream bodies of water. In the midwestern United States, nutrients from small fresh water lakes are carried downstream to other receiving waters such as the Great Lakes, the Mississippi river, and finally to the Gulf of Mexico. The accumulation of excess nutrients in these downstream receiving waters will also trigger algae blooms that in turn create hypoxic dead zones where no fish can live. Such dead zones appear regularly in the Gulf of Mexico, Baltic sea, East China sea, the Kattegat, and along the Oregon coast [24]. These dead zones disrupt the fisheries supported by these bodies of water and so there is tremendous interest in finding ways to restore eutrophic systems to their pristine state.

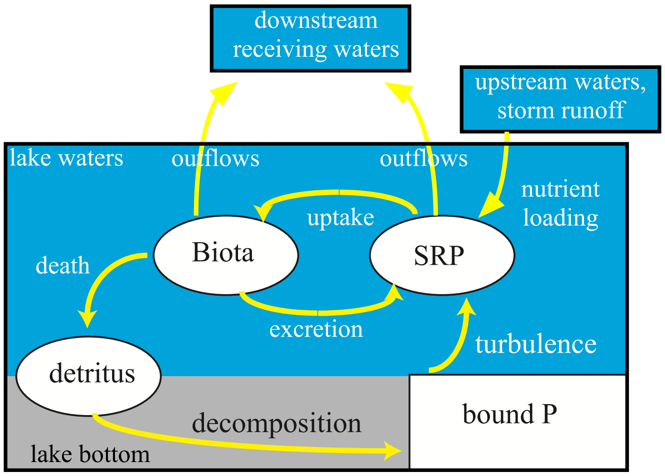

FIGURE 3. Phosphorus cycle in shallow lakes

It is notoriously difficult to restore a eutrophic non-vegetated lake to its pristine state [94]. Simply reducing lake nutrient levels will not trigger a shift back to the clear state due to the way phosphorus cycles through the system. Phosphorus is a critical nutrient for lake vegetation that is taken up by plants as soluble reactive phosphorus (SRP) and used to create plant biomass. This phosphorus rich biomass falls to the lake bottom as detritus when the plant dies. Subsequent decomposition of the detritus allows the phosphorus to adsorb to lake bottom sediments. In general this sediment bound phosphorus is not bio-available. But if the water column's nutrient concentration is low enough or if turbulence mixes lake sediments into the water column, then the bound phosphorus desorbs back into the water column water where it is again taken up by lake vegetation. The fate of phosphorus in the lake may be visualized by the *phosphorus cycle* shown in Fig. 3. The key thing to note in Fig. 3 is that the SRP concentration is governed multiple fluxes; an exchange with the biota, nutrient loading from external sources, outflows to downstream receiving waters, and finally a flux from the lake sediments. It is the interaction of these fluxes into the SRP compartment that give rise to regime shifts in eutrophic lakes.

One may mathematically model the mechanisms driving lake eutrophication as a compartmental system [**61, 46**]. Such systems consist of several *compartments* that are interconnected through fluxes of energy or mass. In particular, each compartment has a local state whose time rate of change is equal to the fluxes entering and exiting the compartment. The inter-compartmental flux is generally a function of the local states in the compartments. The phosphorus cycle in Fig. 3 graphically portrays the compartmental system as a directed graph whose vertices are the compartments and whose edges are the inter-compartmental fluxes. In Fig. 3, one sees four compartments within the lake; biota, SRP, detritus, and bound P. There are two external compartments (upstream and downstream waters) representing sources and sinks for the system. The state of each lake compartment is taken as either nutrient concentration or biomass. The fluxes between compartments are shown by the yellow edges.

A number of compartmental models [21] have been formulated for the cycle shown in Fig. 3. But a particularly simple one was used in [12] to explain lake eutrophication. This model had a single nutrient compartment whose local state, $P : \mathbb{R} \to \mathbb{R}_{\geq 0}$ represents an SRP trajectory that satisfies the following ordinary differential equation,

$$\dot{P}(t) = w(t) - \alpha P(t) + \frac{P^3(t)}{\theta^3 + P^3(t)} \tag{1}$$

where α, θ are positive constants. The first term on the right hand side (RHS) of equation (1) is an input function $w : \mathbb{R} \to \mathbb{R}_{\geq 0}$ representing the total influx of phosphorus from external sources. This is also called the *external loading* term. The second term on the RHS of the equation represents the outflows of water from the lake. The final term in the equation models the influx from sediment bound phosphorus back into the water column. This term is called the *internal loading* term.

The RHS of equation (1) is plotted in the middle panel of Fig. 4. The solid line in this plot is for a constant "nominal" external load $w(t) = w_0$. The internal loading term has a sigmoidal nonlinearity that gives rise to two stable system equilibria shown by the shaded bullets. The left most equilibrium is associated with a pristine lake whose waters are clear (see picture on left side of figure). The right most equilibrium is associated with a eutrophic lake whose waters are clouded by algae (see picture on right side of figure). The region of attraction (ROA) for each stable equilibrium is shown by the shaded regions; with the green region representing the pristine regime and the red region representing the eutrophic regime. The graph in Fig. 4 can be used to identify two distinct regime shift mechanisms; *shock-induced* and *bifurcation-induced* regime shifts.

Shock-induced regime shifts are triggered by impulsive shocks to the system. To illustrate this shock-induced shift on Fig. 4, let us assume the initial lake state, $P(0)$, is in the pristine regime with a baseline external load of

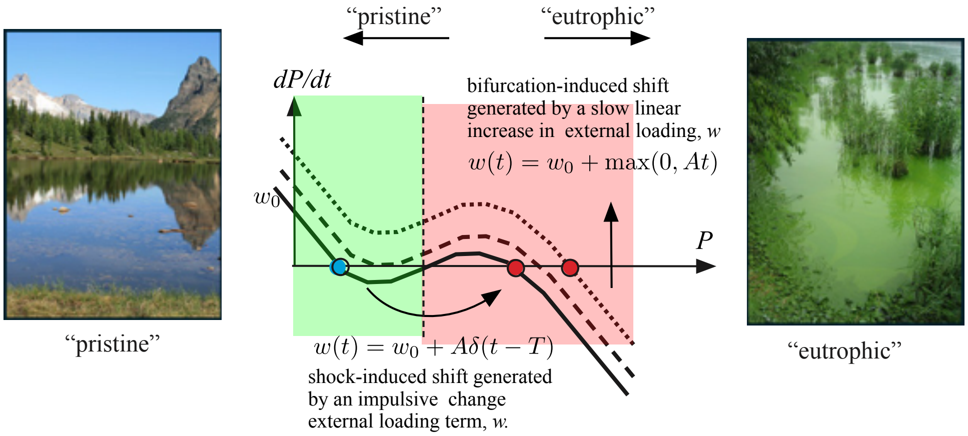

"pristine"

"eutrophic"

FIGURE 4. Eutrophication of Shallow Lake Systems

w_0. A shock-induced shift occurs when a pulse of nutrient is delivered to the lake. Such pulses may occur as a result of extreme rain events that increase runoff from agricultural fields for a short interval of time. We may model the nutrient pulse from a storm that hits at time T as

$$w(t) = w_0 + A\delta(t-T)$$

where $A > 0$ is the size of the pulse and δ is a Dirac impulse function. The delivery of this nutrient pulse at time instant T causes the system state, P, to jump by the amount A as shown in Fig. 4. If that jump places the state in the ROA of the eutrophic equilibrium then the state remains in the eutrophic regime for all $t > T$ and we say a *shock-induced* regime shift has occurred. The minimum pulse amplitude, A, that drives the system into the eutrophic regime may be taken as a threshold whose size provides a measure of how vulnerable the system is to eutrophication caused by nutrient pulses.

Bifurcation-induced regime shifts are triggered by slow variations in the system parameters that cause a topological change in the trajectories satisfying the system's differential equation. Consider, for example, the following slow linear increase in the external loading term of equation (1)

$$w(t) = w_0 + \max\{0, At\}$$

where the linear increase begins at time $t = 0$ and proceeds at a slow rate $A \ll 1$. Now consider the system trajectory over the two intervals $[t_0 - \delta, t_0$ and $[t_0, t_0 + \delta]$ where $\delta > 0$. For most initial times, t_0, there will be a smooth invertible map between the trajectory over $[t_0, t_0 + \delta]$ and the trajectory over $[t_0 - \delta, t_0]$. But there are certain initial times, say t_0^*, where no such invertible map exists. This time represents an abrupt change in the system's behavior that is the result of a *bifurcation* of the system trajectories. This abrupt change in qualitative behavior also represents a regime shift, but the mechanism triggering the shift is qualitatively different from the mechanism behind a shock-induced shift since it is caused by a change in the topology of the system trajectory, rather than a jump in the system state. We therefore refer to this particular regime shift as a bifurcation-induced regime shift.

Fig. 4 can also be used to graphically illustrate the mechanism behind a bifurcation-induced regime shift. In particular, the slow linear increase in the external loading term, $w(t)$, causes the solid curve in the plot to move up. For t close to zero, the pristine equilibrium remains stable, but at the threshold time t_0^*, the system trajectory changes abruptly because of a qualitative change in the system equilibria. In particular, when $t = t_0^*$, the RHS of the differential equation (dashed line) shows that the pristine equilibrium is now only marginally stable. Moreover for $t > t_0^*$ (dotted plot) the pristine equilibrium vanishes entirely and only the eutrophic equilibrium remains stable. This means that for $t > t_0^*$, the system state, P will asymptotically approach the eutrophic equilibrium and the lake will shift into a eutrophic state.

2. Regime Shifts in a Living System

The eutrophication model in equation (1) is highly idealized and ignores the impact of the living compartments (what we call the biota) on the fate of phosphorus. A more complete model capturing the interactions between the nutrient and biotic compartments may be found in a predator-prey system studied in [**37**] and [**112**]. This system still exhibits eutrophication but its behaviors are no longer confined to fixed point convergence and it is a *living* system whose model has been experimentally validated through experiments with a biological chemostat. This section uses that living system to provide a concrete example of regime shifts involved in the collapse and restoration of the system's nominal regime.

A chemostat is a continuous culture device used to study the dynamics of nutrient limited micro-organisms [**104**]. The chemostat's physical set up, shown in Fig. 5(a), consists of three interconnected vessels; a feed, culture, and collecting vessel. The feed vessel holds a liquid media containing all nutrients required for micro-organism growth. All nutrients are available in excess, except for one whose concentration in the feed vessel is denoted as N_{in}. By limiting this nutrient, one can study how variations in nutrient concentration affect the growth of the cultured organisms. In particular, one controls the nutrient's concentration in the culture vessel by adjusting the flow rate of media from the feed vessel into the culture vessel. The volume of the media in the culture vessel is kept constant by setting the outflow rate from the culture vessel into the collecting receptacle equal to the flow rate entering the culture vessel from the feed vessel. A continuous stirrer is used in the culture vessel to ensure the media is well mixed.

The *control variable* that the experimenter uses in the chemostat is the *dilution rate*. Let V denote the constant volume of the media in the culture vessel and let $F(t)$ denote the flow rate of media into and out of the culture

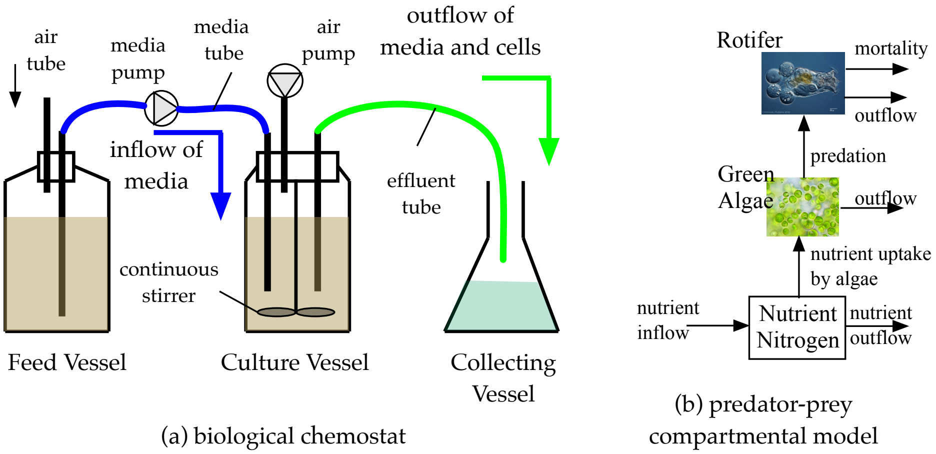

(a) biological chemostat

(b) predator-prey compartmental model

FIGURE 5. (a) Biological Chemostat (b) Predator-Prey Food Web

vessel at time instant t. This flow rate is controlled by the media pump shown in Fig. 5(a). The dilution rate, $\delta(t) = F(t)/V$ at time instant t is the ratio of the flow rate normalized by volume and represents the control input to this particular system.

The micro-organisms in the culture vessel consist of green algae and a planktonic consumer (predator) known as a rotifer. Together these organisms form a live predator prey system [37] that can be modeled as a compartmental system consisting of three compartments; a producer (algae), consumer (rotifer), and nutrient (phosphorus) compartment as shown in Fig. 5(b). *Producers* are micro-organisms, like green algae, that create biomass through photosynthesis. In this case, the growth rate in the producer compartment is limited by the availability of the limiting nutrient. *Consumers* are micro-organisms, like planktonic rotifers, that create biomass through the consumption of other organisms. In this case, the rotifers consume algae as prey and so the consumer's rate of growth is dependent on the algae concentration.

Each compartment in this system has a local state. The nutrient compartment's local state, $N : \mathbb{R} \rightarrow \mathbb{R}_{\geq 0}$, is the nutrient's concentration in the culture vessel. The producer compartment's state, $P : \mathbb{R} \rightarrow \mathbb{R}_{\geq 0}$, is the algae concentration in the culture vessel. The consumer compartment's local state, $C : \mathbb{R} \rightarrow \mathbb{R}_{\geq 0}$, is the concentration of rotifers. Because of the way the chemostat was engineered, the time variations of these states are well modeled by the set of differential equations in Fig. 6 where b_c, k_c, η, b_b, k_b and m are system parameters that are identified through maximum likelihood methods. The nutrient concentration in the feed vessel is a constant N_{in} and the dilution rate $\delta : \mathbb{R} \rightarrow \mathbb{R}_{\geq 0}$ is the controlled input signal.

$$
\begin{aligned}
\dot{N}(t) &= \text{flux in } N \text{ compartment} + \text{flux from feed vessel} \\
&\quad -\text{flux to collection vessel} \\
&= -\frac{b_c N(t)}{k_c + N(t)} P(t) + \delta N_{\text{in}} - \delta N(t) \\
\dot{P}(t) &= \text{flux due to reproduction} \\
&\quad -\text{flux due to predation} - \text{flux to collection receptacle} \\
&= \frac{b_c N(t)}{k_c + N(t)} P(t) - \eta \frac{b_b P(t)}{k_b + P(t)} C(t) - \delta P(t) \\
\dot{C}(t) &= \text{flux due to predation} \\
&\quad -\text{loss due to mortality} - \text{flux to collection vessel} \\
&= \frac{b_b P(t)}{k_b + P(t)} C(t) - mC(t) - \delta C(t)
\end{aligned}
$$

FIGURE 6. State Equations for Fussmann Predator-Prey System [37]

The differential equations in Fig. 6 model mass balance relationships between the three compartments. In other words, the time rate of change of a compartment's local state is equal to the sum of the fluxes entering and exiting that compartment. The physical flux entering the nutrient compartment in the culture vessel is $\delta(t)N_{\text{in}}$ where $\delta(t)$ is the flow rate and N_{in} is the limiting nutrient's concentration in the feed vessel. The physical flux leaving each compartment of the feed vessel is that compartment's local state times the flow rate, $\delta(t)$. The flux entering the consumer compartment due to predation has a Michaelis-Menten mass action kinetic,

$$\text{flux entering } C \text{ compartment due to predation} = \frac{b_c P(t)}{k_c + P(t)} C(t),$$

which models the fact that the consumer's functional response levels off for large producer concentrations. This flux entering the C compartment is balanced by a flux leaving the P compartment

$$\text{flux exiting } P \text{ compartment due to predation} = -\eta \frac{b_c P(t)}{k_c + P(t)} C(t)$$

where η models the feeding efficiency of the consumer. The fluxes connecting the N and P compartments model the fact that the producer's growth rate is dependent on the nutrient concentration and follows a similar mass balance kinetic. These particular dynamical relationships were empirically validated in [**37**] to accurately predict the onset of Hopf bifurcations in live algae-rotifer systems implemented on a biological chemostat.

The differential equations in Fig. 6 may be used to simulate what happens to the food web under various input flow rates, δ. Since this particular model has been experimentally validated, these simulation results should accurately predict what would be seen in the living system. The biotic parameters for the validated system (see chapter 6 of [**112**]) were $b_c = 3.3$, $k_c = 4.3$, $b_b = 2.25$, $k_b = 15$, $\eta = 4$, and $m = 0.1$. The nutrient concentration in the feed vessel is fixed at $N_{\text{in}} = 10$ and we treat the dilution rate, δ, as the "control" that we use to deliver a pulse of nutrient into the system. We initially set this dilution rate to

$$\delta(t) = \begin{cases} 0.1 & t < 100 \\ 2 & 100 < t < 120 \\ 0.1 & 120 < t \end{cases}$$

The objective is to see how the producer and consumer compartment states change in response to the nutrient pulse.

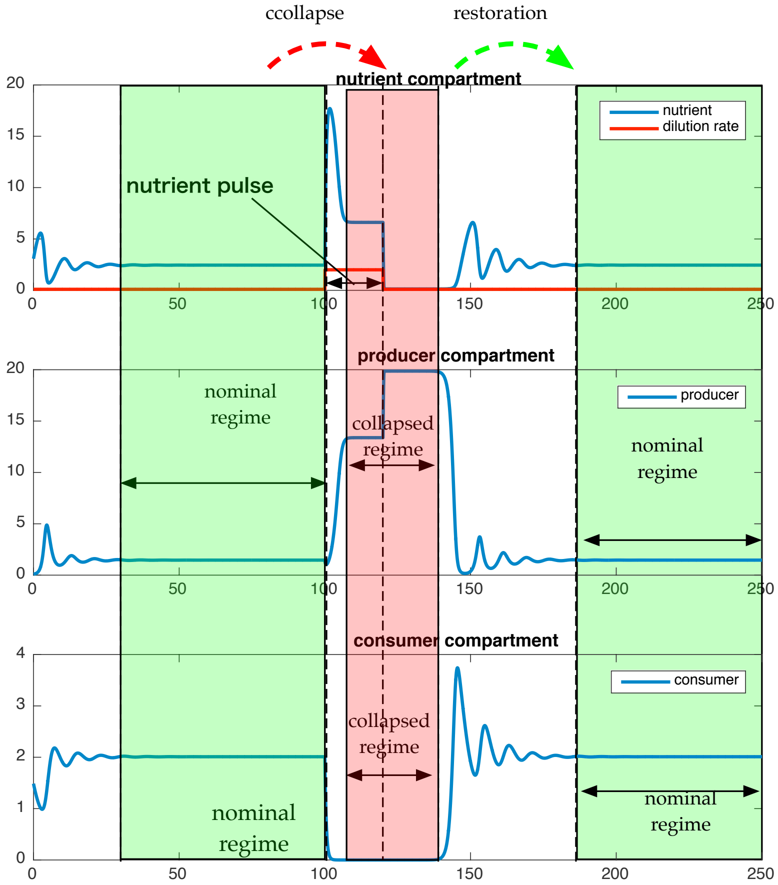

FIGURE 7. Simulation Results for Chemostat System with nutrient pulse from $100 - 120$ time units

Fig. 7 plots the simulated state trajectories for the nutrient, producer, and consumer compartments. There is an initial transient when the simulation starts. By day 25 the compartments have settled to the nominal equilibrium point. The nutrient pulse starts at $t = 100$ and causes an abrupt increase in the culture vessel's nutrient concentration which quickly converges to a steady-state value once the producers begin consuming the excess nutrient. During this time interval the consumer concentration falls to nearly zero because the dilution rate, δ, used to generate the nutrient pulse is large enough so that consumers are being flushed out of the system faster than they can reproduce. In terms of a real world scenario, this simulation may be said to represent lake eutrophication due to increased external nutrient loading. In particular, we see that the jump in external loading at $t = 100$ causes a shift in the system in which producer compartment saturates (i.e. an algae bloom).

Fig. 7 also shows what happens when we try to reverse the algae bloom by reducing the nutrient inflows back to their original value. In particular, we return the dilution rate to its initial value for $t > 120$ days. We see, however, that the compartments do not immediately return to their original levels. In fact once the dilution rate is set back to 0.1, we see producer levels *rise* as a result of decreased flow through the culture vessel and the consumer compartment actually collapses to near zero until $t \approx 140$ days. It is only for time after 140 days that the consumer population grows to a level from which they can graze the producers back to their initial non-eutrophic level. What this time history suggests is that restoring a system back from its eutrophic state is not a reversible process. Full recovery of the pre-eutrophic regime requires the system to traverse a sequence of intermediate regimes that form what was referred to earlier as an *order of succession*.

3. Food Webs with Consumer-Resource Interactions

The predator-prey system in the preceding section was modeled as a compartmental system with *consumer-resource* interactions [**124**]. Such models are commonly used by ecologists to build simulation models that study the impact of fisheries on lake ecosystems [85]. They have also been validated against real-life lake systems [8, 47]. This section shows that these consumer-resource systems often exhibit non-equilibrium behaviors that do not fit easily within the equilibrium-based regime shifts of [97].

Compartmental models for ecosystem food webs model each species in the web as a compartment. The species are also referred to as *guilds*. The local state of a compartment is the biomass of its associated guild. A guild is classified as a *producer* if it does not consume other guilds to create biomass. A guild is classified as a *consumer* if it creates biomass by consuming other guilds. A consumer's consumption rate is a nonlinear sigmoidal function of the resources in its *resource pool*; i.e. the set of all guilds it consumes.

Let $N = \{1, 2, \ldots, n\}$ denote a set of n guilds and let $N_p \cup N_c = N$ denote a partition of these guilds into *producers*, N_p, and *consumers*, N_c. For any guild $i \in N$, we define its *resource pool*, $\mathcal{R}_i \subset N$ as those guilds that are consumed by guild i. The resource pool, $\mathcal{R}_i$, will be empty if i is a producer and is non-empty if i is a consumer. In a similar way, it will be convenient to define a *consumer pool*, $\mathcal{C}_i \subset N_c$, as those guilds consuming guild i.

Each guild has a local state. The ith guild's state trajectory, $x_i : \mathbb{R} \rightarrow \mathbb{R}_{\geq 0}$ takes values $x_i(t)$ representing how much "biomass' is in that guild at time t. For producer guilds ($i \in N_p$), the local state's trajectory satisfies the following ordinary differential equation

$$\dot{x}_i(t) = r_i \left(1 - \frac{x_i}{K_i} \right) - \sum_{k \in \mathcal{C}_i} r_k x_k \frac{x_i}{1 + \sum_{\ell \in \mathcal{R}_k} x_\ell} \tag{2}$$

where r_i is the ith guild's *growth rate* and K_i is a parameter representing the producer's *carrying capacity*. For consumer guilds ($i \in N_c$) the local state trajectory satisfies the differential equation

$$\begin{aligned}\dot{x}_i &= -m_i x_i + \sum_{k \in \mathcal{R}_i} \eta r_i x_i \frac{x_k}{1 + \sum_{\ell \in \mathcal{R}_k} x_\ell} \\ &\quad - \sum_{k \in \mathcal{C}_i} r_k x_i \frac{x_k}{1 + \sum_{\ell \in \mathcal{R}_k} x_\ell}\end{aligned} \tag{3}$$

where m_i is the guild's *mortality rate*, η is the consumer's *feeding efficiency* and the other constants and functions are as defined above for the producer equation.

Not all systems satisfying equations (2) and (3) are biologically plausible. To be biologically plausible the trophic relationships (i.e. who eats whom) and the value of the system parameters must conform to what is observed in real life. Ecologists ensure the biological plausibility of the model by forming trophic relationships in accordance with a niche model [**122**] and by allometric scaling of system parameters such as growth rate, carrying capacity, and mortality rate [**10, 102**]. The niche model randomly assigns a *niche value* to each guild that may be taken as the average body mass of the guild. For each guild, the model randomly generates an interval of niche values that can be consumed by that guild. This model has been shown to be consistent with several real-life food webs [**122**].

The predator-prey model in Fig. 6 is a specific example of a consumer-resource system. The procedure used by the niche model, however, can also be used to randomly generate arbitrarily large model food webs that may be seen as biologically plausible [**122**]. One such food web is shown in Fig. 8. This randomly generated consumer-resource system is a 6 guild food web with a single producer and five consumer guilds. A directed graph showing the trophic relationships between the guilds is shown on the left side of the figure and the system equations are seen in the middle of the figure. The simulated trajectories on the right side of the figure show a behavior that is dominated by interacting recurrent orbits that are consistent with a non-equilibrium dynamical system.

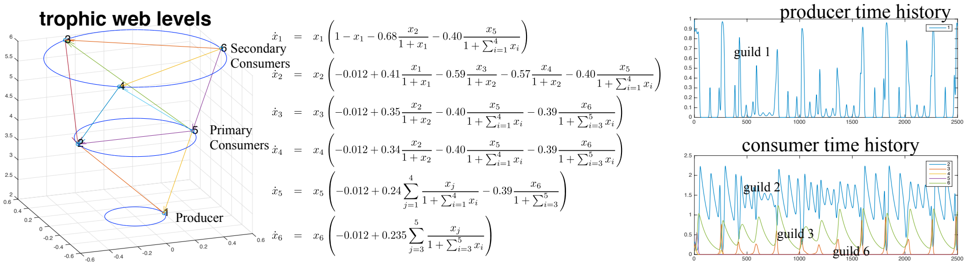

$$\begin{aligned}
\dot{x}_1 &= x_1\left(1 - x_1 - 0.68\frac{x_2}{1+x_1} - 0.40\frac{x_5}{1+\sum_{i=1}^4 x_i}\right)\\
\dot{x}_2 &= x_2\left(-0.012 + 0.41\frac{x_1}{1+x_1} - 0.59\frac{x_3}{1+x_2} - 0.57\frac{x_4}{1+x_2} - 0.40\frac{x_5}{1+\sum_{i=1}^4 x_i}\right)\\
\dot{x}_3 &= x_3\left(-0.012 + 0.35\frac{x_2}{1+x_2} - 0.40\frac{x_5}{1+\sum_{i=1}^4 x_i} - 0.39\frac{x_6}{1+\sum_{i=3}^5 x_i}\right)\\
\dot{x}_4 &= x_4\left(-0.012 + 0.34\frac{x_2}{1+x_2} - 0.40\frac{x_5}{1+\sum_{i=1}^4 x_i} - 0.39\frac{x_6}{1+\sum_{i=3}^5 x_i}\right)\\
\dot{x}_5 &= x_5\left(-0.012 + 0.24\sum_{j=1}^{4}\frac{x_j}{1+\sum_{i=1}^4 x_i} - 0.39\frac{x_6}{1+\sum_{i=3}^5}\right)\\
\dot{x}_6 &= x_6\left(-0.012 + 0.235\sum_{j=3}^{5}\frac{x_j}{1+\sum_{i=3}^5 x_i}\right)
\end{aligned}$$

FIGURE 8. Randomly Generated Consumer-Resource Networks with 6 guilds - (left) trophic relations (middle) system equations (right) steady state trajectories

4. Non-equilibrium Regime Shifts

The equilibrium-based regime shifts depicted in Fig. 2 are too restrictive to describe the behavior of food webs that have periodic or chaotic orbits. The simulated trajectories shown in Fig. 8 exhibit distinct non-equilibrium behaviors for which it is unclear how one might associate a "stable" equilibrium with a given regime. This observation suggests we need a more general way of characterizing system regimes. This section addresses that issue by defining regimes with respect to strongly connected components of the system's positive limit set, what is sometimes called a *Morse decomposition* of the limit set. This paper refers to shifts between these components as *non-equilibrium regime shifts*.

To define precisely what is meant by a Morse decomposition, we first assume that the system equations,

$$\dot{x}(t) = f(x(t))$$

generate unique compact and continuous trajectories. This means that the dynamical system may be characterized by an ordered pair (X, ϕ) where $X \subset \mathbb{R}^n$ is called the *state space* and $\phi : \mathbb{R} \times X \to X$ is a continuous map such that for any $p \in X$ and all $s, t \in \mathbb{R}$, we know $\phi(s+t, p) = \phi(s, \phi(t, p))$ and $\phi(0, p) = p$. It will be convenient to introduce two partial maps of ϕ. The first partial map $\Phi_t : X \to X$ is called the system's *flow*. This map takes values $\Phi_t(p) = \phi(t; p)$ for some fixed $t \in \mathbb{R}$ and all $p \in X$. The second partial map $x(\cdot; p) : \mathbb{R} \to X$ is called a system *orbit* (a.k.a. trajectory). This map takes values $x(t; p) = \phi(t; p)$ for a fixed $p \in X$ and any $t \in \mathbb{R}$. Orbits that are restricted to $t \geq 0$ are called *forward orbits* and those restricted to $t \leq 0$ are called *backward orbits*.

A subset $S \subset X$ of the state space is said to be *invariant* if for any $p \in S$, $\phi(t; p) \in S$ for all $t \in \mathbb{R}$. If for any $p \in S$, we know $\phi(t; p) \in S$ for all $t \geq 0$, then S is *positively invariant*. In a similar way, the restriction that backward orbits starting at $p \in S$ remain in S implies S is *negatively invariant*. We will assume throughout that the orbits of the system are compact (closed and bounded sets in $\mathbb{R}^n$). For our applications, this is not an unreasonable requirement since the local state (population size) of all compartment in a living system must remain bounded. If all orbits of (X, ϕ) are compact then there must exist an invariant set S such that the restriction of the flow to S is an automorphism; i.e. $\Phi_t : S \to s$ for all $t \in \mathbb{R}$. Given a system (X, ϕ) with compact orbits, we're interested in characterizing the set of all *chain recurrent states* (i.e. states that are returned to infinitely often) since we will use this set to define the system's regimes.

An ϵ-chain from $p \in X$ to $q \in X$ is a finite sequence $\{(x_k, \tau_k)\}_{i=1}^{N}$ of points in $X \times \mathbb{R}$ such that $N \geq 2$, $x_1 = p$, $x_N = q$ and

$$|x_{k+1} - \phi(\tau_k, x_k)| < \epsilon$$

The ϵ-chain is a sequence of points that more closely tracks an orbit of a dynamical system as ϵ goes to zero. If we consider an ϵ-chain from p back to itself, we can obviously periodically extend this chain to create an infinite length *periodic* ϵ-chain.

Let $S \subset X$ be a compact positively invariant set of the system and consider two sets $A, B \subset S$. We define $\mathrm{ch}_\epsilon(A, B; S)$ as the union of all ϵ-chains in S that start in A and end in B. We say a state $p \in S$ is *ϵ-chain recurrent* if $\mathrm{ch}_\epsilon(p, p; S)$ is nonempty and we let

$$R_\epsilon(S) = \{p \in S \,:\, \mathrm{ch}_\epsilon(p, p; S) \text{ is nonempty}\}$$

denote the *ϵ-chain recurrent set* with respect to compact set $S \subset X$. The system's *chain recurrent set*, $R(S)$, with respect to compact $S \subset X$ is then defined as the intersection of all its ϵ-chain recurrent sets

$$R(S) = \bigcap_{\epsilon > 0} R_\epsilon(S)$$

Long term steady state behaviors of the system are contained in its *positive limit set*. Given any point $p \in S$, we say q is a positive limit point of p if there is an infinite sequence $\{\tau_k\}_{k=1}^{\infty}$ such that $\tau_k \to \infty$ as $k \to \infty$ and $\lim\limits_{\tau_k \to \infty} \phi(\tau_k; p) = q$. The set of all positive limit points of p is denoted as $\omega(p)$ and the set of all positive limit sets for the compact set $S \subset X$ is denoted as $\Omega(S) = \bigcup\limits_{p \in S} \omega(p)$. An important fact is that the positive limit set of S is contained within the system's chain recurrent set $R(S)$.

Given any two points p, q in the chain recurrent set $R(S)$, we can introduce a binary relation that says $p \sim q$ if and only if for all $\epsilon > 0$ there exists a periodic ϵ-chain containing p and q. One can easily show that this binary relation is an equivalence relation which means the chain recurrent set can be decomposed as the union of mutually exclusive equivalence classes. In particular, we denote the equivalence class that a point $p \in R(S)$ lies in as $[R(S)]_p$. These equivalence classes are called *basic sets*. Note that because the system's positive limit set $\Omega(S)$ is contained within $R(S)$, this means that the positive limit set of the system can also be decomposed with respect to the basic sets of $R(S)$ by simply taking the intersection of $\Omega(S)$ with each of the basic sets $\{[R]_p(S)\}$. We will denote these "basic" sets for the positive limit set as $[\Omega]_p(S)$ where p is some state in $\Omega(S)$. One can use a result known as Conley's decomposition theorem [**14**] to place a partial order on these basic sets. Ordered decompositions of invariant sets are sometimes called *Morse decompositions* and so the basic sets of $\Omega(S)$ can also be referred to as a Morse decomposition of the positive limit set.

Let us consider a dynamical system (X, ϕ) where S is the largest compact invariant set in X. Since we know the system's positive limit set $\Omega(S)$ can be decomposed into a collection of basic sets $[\Omega]_p(S)$, we will define a system *regime* as one of these basic limit sets. A *regime shift* occurs when the system state switches between these basic sets as a result of an external disturbance (i.e. a shock-induced regime shift) or a change in the topology of these basic sets (i.e. a bifurcation-induced regime shift). Note that the regime shift mechanisms are essentially the same as we defined before for the lake eutrophication example, but now the regimes are no longer defined with respect to stable system equilibria. They are defined with respect to a Morse decomposition of the system's positive limit set and this characterization means that the regime shift concept can now be extended to non-equilibrium systems.

Let us now consider a realistic example of a food web whose regimes are defined in terms of the positive limit set's basic sets. We consider a tritrophic extension of the Rosenzweig-MacArthur [**93**] predator prey system. The original Rosenzweig-MacArthur system consists of a producer and a "primary" consumer. This model can be extended to a three guild system by adding a "secondary" consumer that only feeds on the primary consumer. The resulting tritrophic food web shown in Fig. 9(a) assumes the producer is algae, the primary consumer is a planktonic crustacean such as

Daphnia and the secondary consumer is a lake fish such as a black crappie. This simple food web is well known to exhibit a wide range of complex behaviors that include chaotic orbits [**50**].

We model this food web as a non-negative compartmental system with the consumer-resource interactions introduced in the preceding section. The model has three compartments for the producer (x_1), the primary consumer (x_2), and the secondary consumer (x_3). The compartmental states satisfy the following set of differential equations

$$\dot{x}_1 = r_1 x_1 \left(1 - \frac{x_1}{K}\right) - r_2 \frac{x_1 x_2}{\theta_1 + x_1} \tag{4}$$

$$\dot{x}_2 = \eta_2 r_2 \frac{x_1 x_2}{\theta_1 + x_1} - r_3 \frac{x_2 x_3}{\theta_2 + x_2} - m_2 x_2 \tag{5}$$

$$\dot{x}_3 = \eta_3 r_3 \frac{x_2 x_3}{\theta_2 + x_2} - m_3 x_3 \tag{6}$$

where K is the producer's carrying capacity. The parameters r_i, η_i, and m_i denote the growth rate, feeding efficiency and mortality rate of guild i, respectively. The RHS of these equations model fluxes entering and exiting the compartment. The producer equation (4) has two terms; the first term models growth due to photosynthesis and the second term models predation by the primary consumer. The primary consumer equation (5) has three terms; the first term models growth due to predation on the producer, the second term models loses due to predation by the secondary consumer, and the third term models loses due to mortality. The secondary consumer's equation (6) is similar to that of the primary consumer and has only two fluxes; one for mortality and another modeling growth due to predation on the primary consumer.

The tritrophic food web in equations (4-6) is well known to exhibit a range of qualitative behaviors [**50**]. One can switch between these behaviors by simply changing parameter values. Figs. 9(b) and (c), for instance, show

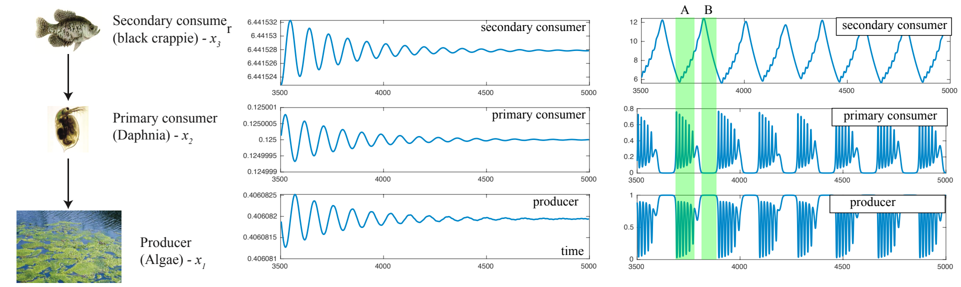

(a) tritrophic food web

(b) carrying capacity, K=2/3

(c) carrying capacity, K=1

FIGURE 9. (a) Tritrophic food web (b) convergence to fixed point (c) bursting

simulated trajectories for two different values of the producer's carrying capacity, K. The simulated orbits in Fig. 9(b) asymptotically converge to a fixed point in the state space. By slightly increasing the carrying capacity, the system orbits qualitatively change as shown in Fig. 9(c) to exhibit a *bursting behavior* where the system is alternating between oscillatory bursts (green region A) and non-oscillatory behavior (red region B). In this case, one may ask whether the system is undergoing regime shifts between behaviors A and B, or if there is only a single "complex" regime?

This section answers that question using our definition for regimes as basic sets of the system's positive limit set. These basic sets can be obtained by looking at the orbits generated by initial states starting in the neighborhood of the system's equilibria. In particular, we computed orbits generated by the following initial states,

$$\begin{aligned} x_{0a} &= (0.0, 1.0, 0.0)^T, & x_{0b} &= (0.01, 0.00, 0.01)^T \\ x_{0c} &= (0.01, 0.01, 0.00)^T, & x_{0d} &= (0.01, 0.01, 0.01)^T \end{aligned}$$

Fig. 10(a) plots the orbits for the case where the selected carrying capacity ($K = 2/3$) only exhibits fixed point convergence. Fig. 10(a) shows that this system's positive limit set consists of four fixed points; each one being a basic set that captures the orbits for specific subsets of initial conditions. Each of these basic sets represent a distinct regime for the system where regime A is a *dead* system, regime B is dominated by the producer (eutrophic regime), regime C has no secondary consumer (no fish), and all three compartments in regime C are positive (live system).

The need for a non-equilibrium characterization of regime shifts is seen in Fig. 10(b). This figure plots the orbits for the system initial conditions when the producer's carrying capacity $(K = 1)$ results in bursting. This figure shows that this system's positive limit set again has four basic sets, but some of these sets now have distinctly different topologies. Regime A is the dead system and regime B is still a fixed point representing the eutrophic state of a producer dominated biota. Regime C is now a limit cycle in which the producer and primary consumer alternate in their dominance of the system biota. The component marked D has a more interesting "teacup" shape associated with bursting. Each of these sets represents a different regime that can "trap" the system's behavior. Recall that we asked earlier whether the bursting behavior in Fig. 9(c) represented two regimes or a single one. If we define a system regime as a basic set of the system's positive limit set, then the answer to our question is that bursting orbits are trapped within a single regime with a very complex topology (teacup shape).

5. Pseudo Regimes

The preceding section defined system regimes in terms of the basic sets of a system's positive limit set. Some may still find this answer unsatisfactory. The bursting behavior in Fig. 9(c) is often described informally as a behavior that periodically generates sustained oscillatory bursts. That description clearly thinks of bursting as a transition between an oscillatory and non-oscillatory regime. If that is not a regime shift, then what is it?

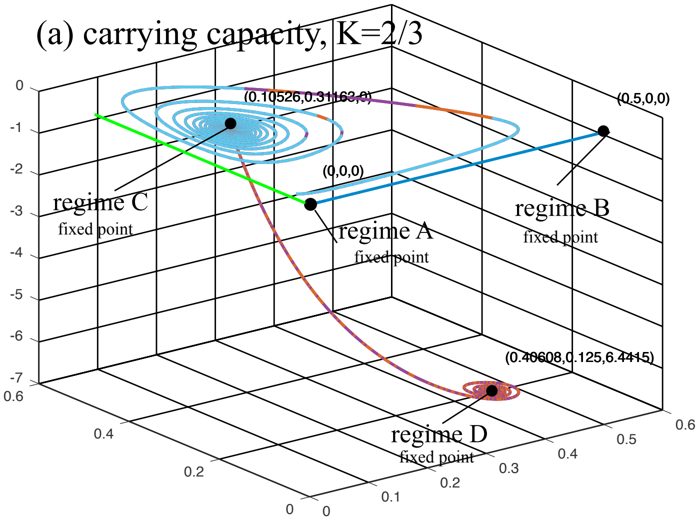

(a) carrying capacity, K=2/3

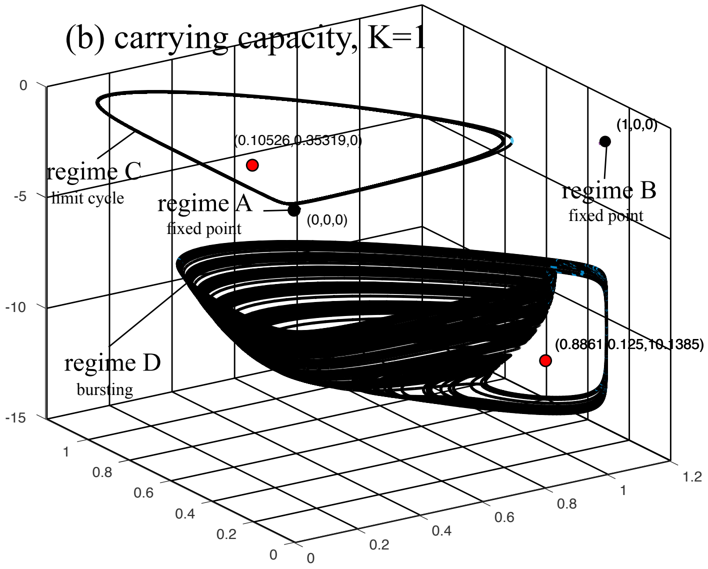

(b) carrying capacity, K=1

FIGURE 10. Morse Decomposition of Positive Limit Set for tritrophic food web (a) equilibrium-based regimes (b) bursting

To answer that question, we note that if two systems, p and q, are in the same basic set (i.e. regime) then there is a periodic ϵ-chain that contains both states. In this regard, we have defined regimes as states that "eventually" communicate with each other. Clearly all states within the same regime communicate with each other. But if we are also concerned with the length of time between successive visits, then this provides a reasonable basis for partitioning the basic set into distinct regions or *pseudo regimes* where the basic set's orbit spends most of its time. On the surface, this type of partition might be used to provide a syntactical explanation for the behavior seen in a "bursting" regime.

One way of forming such a partition is to introduce a probability measure on the transition map, ϕ, so that it becomes a transition probability. The orbits on the basic set would then be random walks of a Markov process whose invariant distribution could be used as a basis for partitioning the basic set in terms of each state's recurrence time. The following example shows how this partition might be constructed from a sufficiently long orbit contained in the basic set.

For example, let $x(\cdot;p) : \mathbb{R} \to S$ denote an orbit of the system where p is in one of the positive limit set's basic sets. Let us sample this orbit in time and space by constructing a grid set

$$\mathcal{G} = \left\{ \left\lfloor \frac{x(kh;p)}{dx} \right\rfloor \right\}_{k=1}^{\infty}$$

for $k = 0, 1, \ldots$ and where h and dx denote denote the sampling interval in time and space, respectively. The grid set, $\mathcal{G}$, is esssentially a cubical gridding of the basic set. To each grid element $\mathcal{G}$, there is a "cube" of points in $\mathbf{R}^n$. The union of all of theses cubes forms a set that is called a *cubical complex*. We use the sample orbit $\{x(kh;p)\}_{k=0}^{\infty}$ to construct a single step transition probability $Q(i|j)$ as the probability that the system being in grid element $j \in \mathcal{G}$ will transition to grid element $i \in \mathcal{G}$ within a fixed window of time. The ordered pair $(\mathcal{G}, Q)$ forms a Markov chain and we are interested in finding a meaningful way of partitioning that grid set, $\mathcal{G}$, based on the recurrence times.

There are many ways such a partition can be obtained, but since we are concerned with clustering states into sets where the orbit spends the most time, it makes sense to construct a partition

$$\mathcal{G} = \mathcal{A} \cup \mathcal{A}^*$$

that minimizes the sum of the probabilities of leaving $\mathcal{A}$ and $\mathcal{A}^*$. This particular problem can be solved using a variant of the `NCUT` algorithm [**101**]. This algorithm takes the Markov chain's directed graph and computes the eigenvector for the second largest eigenvalue of its normalized graph Laplacian. The components of that eigenvector are partitioned into two sets, placing those components with a value greater than a selected threshold into one set and the rest in the other set. Each component of the eigenvector represents, of course, a state in the grid space $\mathcal{G}$, so the partitioning of the eigenvector induces a partition of the Markov chain's grid space, $\mathcal{G}$. The `NCUT` algorithm simply chooses a threshold that minimizes the probability flux between the two components in this partition of the grid space. This approach is computationally tractable and forms the basis for many algorithms used in graph partitioning [**119**].

This procedure was applied to a bursting orbit of the tritrophic food web. The grid size, dx, was chosen so the resulting cubical complex had a persistent topology [**31**] as measured by the complex's Betti numbers [**51**]. The resulting cubical complex is shown in Fig. 11(a). The graph partition that was obtained using the `NCUT` algorithm is shown in Fig. 11(b). The primary partition shown in green has Betti numbers $(1, 1, 0)$, which means the complex has a single connected component with a 1-dimensional hole through it. This topology is consistent with the behavior associated with a periodic oscillation. The second component, shown in red, has Betti numbers

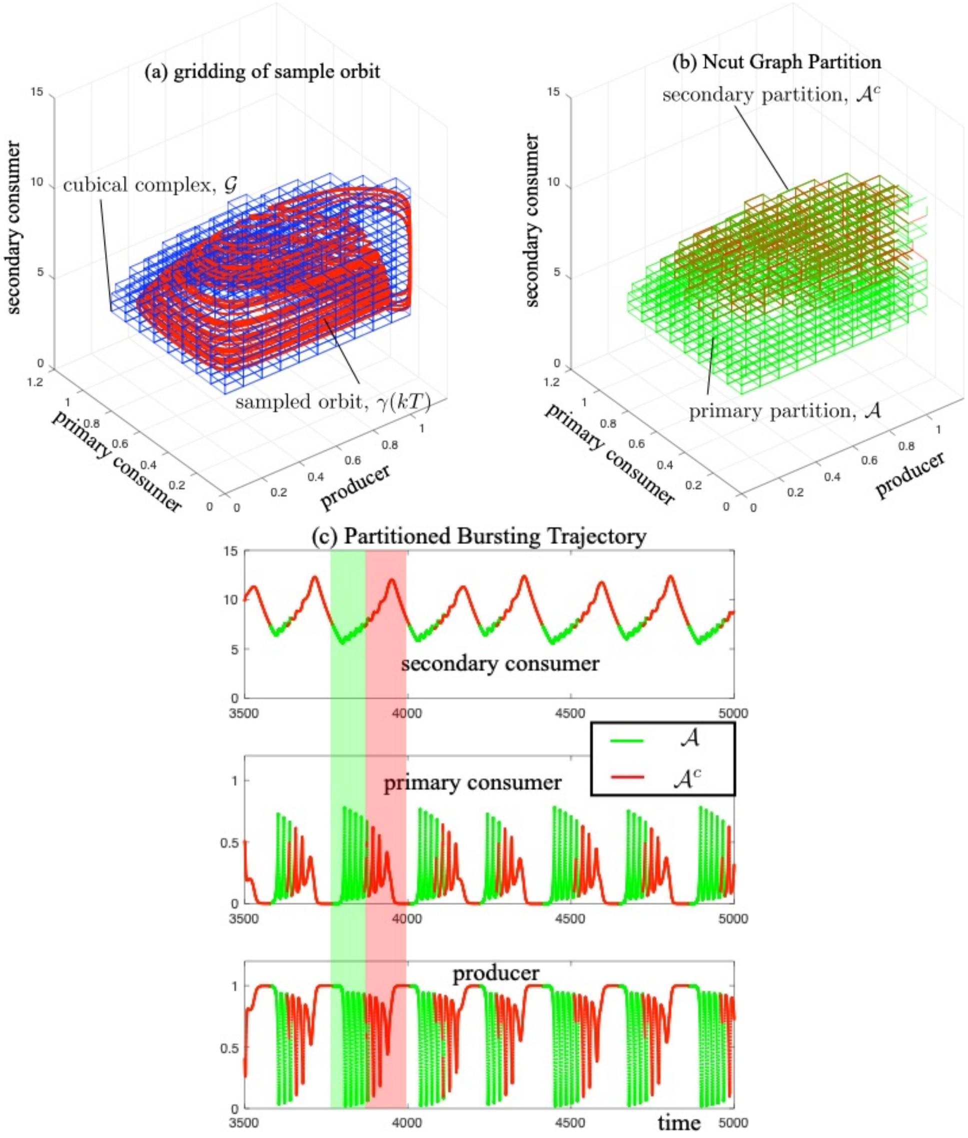

FIGURE 11. Partitioning the Bursting Regime using the NCUT Algorithm

$(1, 0, 0)$ which means there is only a single connected component with no holes. This partition was projected onto the orbit shown in Fig. 11(c) and comparing this back to the regions identified in Fig. 9(c), it should be apparent that the graph partition obtained using `NCUT` is consistent with the informal description that describes bursting as switching between oscillatory and non-oscillatory behaviors.

The preceding partition of bursting orbit, of course, does not represent a decomposition of the orbit into distinctly different basic sets, i.e. regimes. But it is still meaningful from the standpoint of describing the orbit in terms of changes in the orbit topology. The preceding section gave an unambiguous characterization of regimes in terms of the system's "basic" invariant sets. This section showed that this regime concept could also be meaningfully refined in terms of topological invariants. This monograph will not explore the notion of a pseudo-regime any further. The remaining chapters focus on regime shifts between basic sets.

6. Summary and Further Reading

Regime shifts represent a fundamental concept in the study of ecological resilience. These shifts can signal the collapse of a functioning system and they are intentionally triggered to speed up the restoration of a collapsed system. Ecologists usually describe regime shifts using equilibrium concepts (i.e. a transition in the system state between alternative stable equilibria), but real-life food webs, especially those that satisfy consumer-resource interactions, exhibit non-equilibrium behaviors. This chapter rigorously defined *non-equilibrium regime shifts* in terms of the basic sets of the system's positive limit set. The chapter identified two regime shift mechanisms; shock-induced and bifurcation-induced. Shock-induced regime shifts occur when a disturbance forces the system state into an alternative basic set. Bifurcation-induced regime shifts occur when parameter variations change the topology of the basic sets. The chapter closed with a refinement of the non-equilibrium regime shift concept (pseudo-regimes) that used spectral partitions of graphs to partition a basic set based on its topological invariants.

The ecology literature on regime shifts is vast, but often focuses on developing a link between the equilibrium-based picture in Fig. 2 [**97**] and observations [**96**] in real-life systems. This has led to a number of statistical indices used to predict future regime shifts [**75**, **95**, **5**, **18**, **100**] and studies that look for regime shifts in particular ecosystems [**57**, **23**, **80**, **58**, **20**, **11**, **33**]. The recognition of the role of regime shifts in restoration ecology has been examined in [**108**, **109**, **52**]. In spite of the intense interest from ecologists in regime shifts, there has been some skepticism regarding the practical value of the concept in the adaptive management of real life systems [**43**]. This chapter's novelty rests with its formal definition of regime shifts in terms of the basic sets of a consumer-resource system. That definition provides a rigorous way of extending the regime shift concept to non-equilibrium systems.

Complex food webs have long been modeled as compartmental systems [**61**] based on nutrient fluxes [**21**] or metabolic energy [**10**]. The consumer-resource systems cited in this chapter were based on [**124**] with trophic relationships given by the niche model [**122**] using allometrically scaled parameters [**10**, **102**]. Models of this form will be found in simulation tools for fishery management [**85**]. One of the reasons for using such models is that one can randomly generate large biologically-plausible models for food webs. Our confidence in these models rest on prior studies [**8**] that have validated such models against real life lake system.

Topological concepts lay at the heart of the regime-shift definition given in this chapter. This chapter's coverage of chain recurrence and basic sets is drawn from [**30**, **60**]. These concepts will be used in later chapters to discuss

Conley's decomposition theorem [14] that forms the basis for constructing a discrete-abstraction of regime shift dynamics.

The discussion in the final section computed topological invariants (Betti numbers) for cubical complexes containing the basic sets. More detail on these topological invariants may be found in [51]. These topological invariants have recently been used to help refining data sets in a manner that ensures the topology of the resulting sets is persistent [41, 31]. While most of this prior work has focused on the use of simplicial complexes in computing topological invariants, we have that cubical complexes appear easier to work with for data sets generated by dynamical systems. Computational tools used in finding the topological invariants of such cubical complexes will be found in [64].